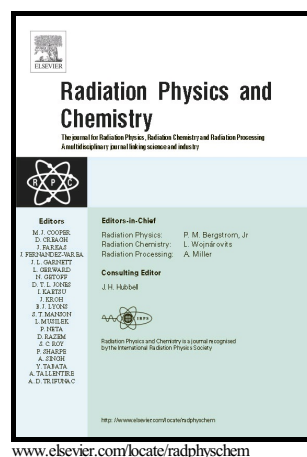


Author's Accepted Manuscript

Calibration and performance of a real-time gamma-ray spectrometry water monitor using a LaBr₃(Ce) detector

E. Prieto, R. Casanovas, M. Salvadó



PII: S0969-806X(17)30636-9
DOI: <https://doi.org/10.1016/j.radphyschem.2017.10.008>
Reference: RPC7667

To appear in: *Radiation Physics and Chemistry*

Received date: 19 June 2017
Revised date: 14 September 2017
Accepted date: 8 October 2017

Cite this article as: E. Prieto, R. Casanovas and M. Salvadó, Calibration and performance of a real-time gamma-ray spectrometry water monitor using a LaBr₃(Ce) detector, *Radiation Physics and Chemistry*, <https://doi.org/10.1016/j.radphyschem.2017.10.008>

This is a PDF file of an unedited manuscript that has been accepted for publication. As a service to our customers we are providing this early version of the manuscript. The manuscript will undergo copyediting, typesetting, and review of the resulting galley proof before it is published in its final citable form. Please note that during the production process errors may be discovered which could affect the content, and all legal disclaimers that apply to the journal pertain.

Calibration and performance of a real-time gamma-ray spectrometry water monitor using a LaBr₃(Ce) detector

E. Prieto¹, R. Casanovas¹ and M. Salvadó¹.

¹ Unitat de Física Mèdica, Facultat de Medicina i Ciències de la Salut, Universitat Rovira i Virgili, ES-43201 Reus (Tarragona), Spain

Abstract

A scintillation gamma-ray spectrometry water monitor with a 2''×2'' LaBr₃(Ce) detector was characterized in this study. This monitor measures gamma-ray spectra of river water. Energy and resolution calibrations were performed experimentally, whereas the detector efficiency was determined using Monte Carlo simulations with EGS5 code system. Values of the minimum detectable activity concentrations for ¹³¹I and ¹³⁷Cs were calculated for different integration times. As an example of the monitor performance after calibration, a radiological increment during a rainfall episode was studied.

Key words: scintillation gamma-ray spectrometry, LaBr₃(Ce), Monte Carlo simulation, efficiency calculation, MDAC

1 Introduction

Ascó nuclear power plant is located in the village of Ascó, Catalonia (ES-E, Spain-East), beside the Ebre river. The water of the river is used for cooling the two pressurised water reactors of the plant. However, this water is also used for human consumption and irrigation of agricultural crops. Therefore, a continuous radiological surveillance of the water of the Ebre river is required.

For this purpose, two real-time water gamma-ray spectrometry monitors with NaI(Tl) detectors, located before and after the river flows through Ascó nuclear power plant were improved, calibrated and tested in a previous study of our research group (Casanovas et al., 2013).

This improvement was part of a more ambitious project where the measurement capabilities of the automatic real-time surveillance network in Catalonia (ES-E, Spain-East) were enhanced using real-time gamma-ray spectrometry. For this, two other type of monitors using either NaI(Tl) or LaBr₃(Ce) scintillation detectors were also developed, calibrated and implemented: an aerosol monitor using a particulate filter (RARM-F) (Casanovas et al., 2014a) and a monitor using two shielded detectors measuring directly to the environment (RARM-D2) (Casanovas et al., 2014b).

The better performance of LaBr₃(Ce) detectors in comparison with NaI(Tl) ones has been clearly observed in both RAMR-F and RARM-D2 monitors. The advantages of LaBr₃(Ce) detectors for environmental monitoring have been widely studied (Toivonen et al., 2008), (Mattila et al., 2010). The better resolution of LaBr₃(Ce) detectors from 100 keV permits the identification of artificial photopeaks of importance for environmental monitoring that are close to natural emissions (Casanovas et al., 2014a). For example, the ¹³¹I emission of 364 keV is

resolved from the 352 keV peak of ^{214}Pb when spectra are obtained with $\text{LaBr}_3(\text{Ce})$ (Toivonen et al., 2008). Moreover, these detectors present a linear energy response, good stopping power and higher light yield than $\text{NaI}(\text{Tl})$ detectors (Quarati et al., 2007), (Menge et al., 2007).

Hence, an improvement in the performance of the river water monitors is also expected if a $\text{LaBr}_3(\text{Ce})$ detector is used instead of a $\text{NaI}(\text{Tl})$ one. In fact, $\text{LaBr}_3(\text{Ce})$ detectors showed good properties when used for marine water monitoring in other studies (Su et al., 2011), (Zeng et al., 2017). In this paper, the measurement capabilities of the river water monitors when using $\text{LaBr}_3(\text{Ce})$ detectors were evaluated. The new system, where the $\text{LaBr}_3(\text{Ce})$ detector was implemented, was calibrated in energy, resolution and efficiency. Minimum detectable activity concentrations (MDAC) were calculated for ^{131}I and ^{137}Cs for different integration times.

2 Materials

2.1 Water Monitor System



Figure 1. Water monitor (left), vessel cover with detector enclosure (middle), vessel with Pb shielding (right)

The river monitor, whose measurement capabilities using a $\text{LaBr}_3(\text{Ce})$ were tested, was the one located upstream of the nuclear power plant, known as North Ebre River Monitor. Due to regulatory issues related to the availability of the river monitors, the time dedicated to study the monitor with a $\text{LaBr}_3(\text{Ce})$ detector was limited. During the trial period, the river monitor located after the nuclear power plant (South Ebre River Monitor) continued functioning with a $\text{NaI}(\text{Tl})$ detector.

The monitor used in this study (see Figure 1) was a Berthold LB/BAI 9110 (Berthold Technologies GmbH & Co. KG, Germany) that was enhanced with different features in a previous study (Casanovas et al., 2013). The original $\text{NaI}(\text{Tl})$ detector was replaced by a 2"×2" $\text{LaBr}_3(\text{Ce})$ from Saint Gobain Crystals®. The detector was connected to a digital multichannel analyser (ORTEC® Digibase) of 1000 channels which was in turn connected to a computer. All collected data are transferred to an external server and stored in a SQL database using an ADSL connection. The system is prepared for remote control of the monitor and interaction with the server through an external computer.

The measurement process begins when the water is collected from the river by a pump. The water flows continuously through a 25 L vessel inside of which the scintillator detector is placed. The vessel and the detector are surrounded by a lead shielding to minimize the external

radiation contribution. In addition, the system is connected to two 15 L water sampling recipients aimed for posterior analysis that can be filled manually and automatically up to a selected level in case of exceeding established radiological criteria. Figure 2 shows a scheme of this process.

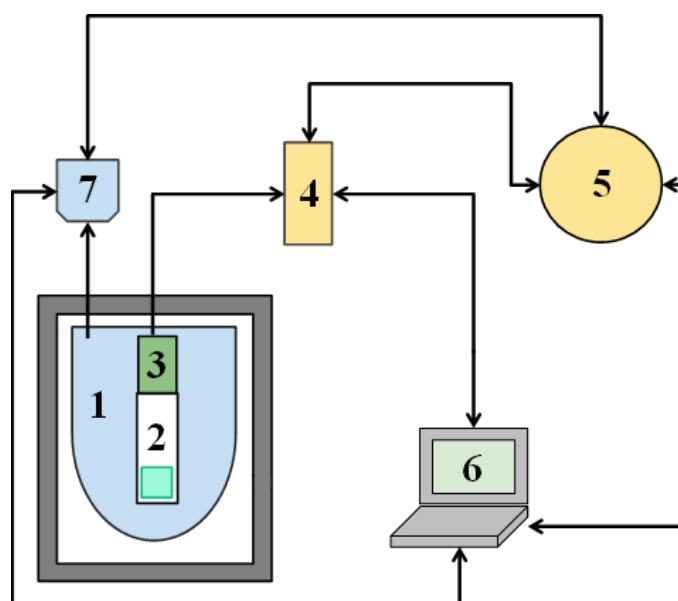


Figure 2. Scheme of the Water Monitor System. (1) vessel; (2) LaBr₃(Ce) detector; (3) digital MCA, (4) local computer; (5) SQL server; (6) external computer; (7) sampling recipients.

The remote control of the system is done via TCP/IP protocol. The system is also equipped with sensors for electronic checking such as a flow meter, a detector temperature probe or a meteorological station measuring wind speed and direction, air temperature, humidity, barometric pressure, rainfall and solar radiation.

2.2 Calibration sources

For calibration purposes, different radioactive sources were used in this study. They encompassed point-sources of ¹⁵²Eu, ¹³⁷Cs and ⁶⁰Co, a hermetically sealed natural source of ²²⁶Ra (with its corresponding ²¹⁴Pb and ²¹⁴Bi daughters) and ¹³⁸La emissions from the self-contamination of the detector LaBr₃(Ce) crystal.

3 Methods

3.1 LaBr₃(Ce) self-activity determination

The typical shape of spectra obtained with LaBr₃(Ce) detectors in low count rate scenarios is due to the presence of radioactive ¹³⁸La and ²²⁷Ac in the detector crystal (Quarati et al., 2012). For analysis purposes, it was convenient to quantify the intrinsic activity arising from the LaBr₃(Ce) detector crystal in a low background environment. For that, the detector was placed inside the water monitor, which is shielded with lead, when the vessel was empty. The absence of any photopeak from natural origin was checked after an integration time of several hours.

3.2 Calibration

3.2.1 Spectra stabilisation

Prior to calibration, the spectra need to be stabilised to correct the peak positions that can be affected by water temperature variations. The stabilisation is performed by fitting two Gaussian curves to the ^{138}La double peak at 1440 keV and 1470 keV to find their position and correct the entire spectrum using the second method described in a previous study (Casanovas et al., 2012a). This process is performed automatically and stabilized spectra are stored into the database.

3.2.2 Energy and resolution calibrations

The applied calibration methodology (Casanovas et al., 2012b) was adapted to the particular characteristics of the water monitor with a $\text{LaBr}_3(\text{Ce})$ detector.

The calculation of the energy and resolution calibrations was performed using the radioactive sources described in Section 2.2. A second-degree polynomial was adjusted to obtain the energy calibration:

$$E = a_0 + a_1 \cdot C + a_2 \cdot C^2 \quad (1)$$

where C is the channel number, E is the energy and a_k are the fitting coefficients.

In order to properly analyse the obtained spectra, it is necessary to perform the resolution calibration. The resolution calibration was determined adjusting the experimental values of the Full Width at Half Maximum (FWHM) to a second-degree polynomial:

$$FWHM(E) = b_0 + b_1 \cdot E + b_2 \cdot E^2 \quad (2)$$

where $FWHM(E)$ is the Full Width at Half Maximum, E is the energy and b_k are the fitting coefficients.

However, the calculation of the FWHM in energy units cannot be simply determined applying equation (1) straightforward. The FWHM was obtained subtracting the energy value of the lower channel to the higher channel determined by Equation (1).

3.2.3 Monte Carlo simulated efficiencies

The efficiency calibration was determined using Monte Carlo (MC) simulations with the EGS5 user code that was previously validated (Casanovas et al. 2012). The information regarding the diluted radiation source, the geometry (shape and dimensions) and materials of the system (e.g. vessel, shielding, detector, detector water around the detector, etc.) was implemented into the code. Thus, a model of the monitor based on the real characteristics was simulated. The density and composition of the monitor materials were taken from Berger et al. (2005). The modelled monitor is shown in Figure 3. The simulated radiation was set at a cut-off energy of 10 keV for photons and electrons.

Each point of the efficiency curve was calculated considering a monoenergetic source in the range of 20 to 2000 keV distributed homogeneously in the water volume. The obtained spectra

for the simulated monoenergetic sources were convoluted with the resolution function obtained with Equation (2) by using the method described in a previous study (Casanovas et al. 2012). After that, the broadened spectra were used to calculate the efficiencies using the spectra analysis software ScintiVision™ from ORTEC®.

The efficiency was calculated as:

$$\varepsilon_{MC} = \frac{N_{counts}}{N_{hist}} \quad (3)$$

where N_{counts} is the number of net counts under the full energy peak and N_{hist} is the number of simulated histories (i.e. the number of primary source-particles simulated and all of the secondary particles produced by it), which was set at 10^7 .

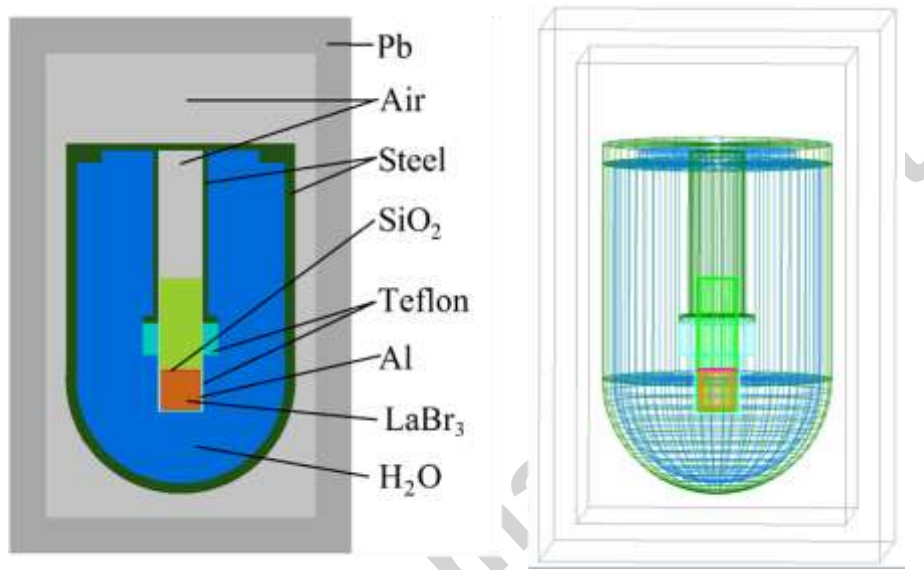


Figure 3. Implemented geometry model and materials for the MC efficiency simulation.

The efficiency calculations were fitted to the following function:

$$\log \varepsilon_v = \sum_{n=0}^6 a_n (\log E)^n \quad (4)$$

where ε_v is the volumetric efficiency at the gamma-ray energy E and a_n represents the fitting coefficients.

3.3 Activity Concentration and Minimum Detectable Activity Concentration (MDAC)

The activity concentration (e.g. Bq L⁻¹) related to each peak can be written as:

$$a = \frac{N}{\varepsilon_v \cdot t \cdot p_\gamma} \quad (5)$$

where N is the number of counts under the peak, t the counting time, p_γ is the emission probability of the gamma-ray and $\varepsilon_V \equiv \varepsilon \cdot V$ is the volumetric efficiency, where ε is the peak-efficiency and V is the volume of the vessel, which was 25 L in this study.

The Minimum Detectable Activity Concentration corresponds to the activity measured from the detection limit, L_D . The detection limit is the minimum number of counts under a peak that one can be confident of detecting with a certain probability.

From Equation (5) the MDAC can be determined as:

$$MDAC = \frac{L_D}{\varepsilon_V \cdot t \cdot p_\gamma} \quad (6)$$

where the detection limit L_D (with a 95% confidence limit) for a certain Region of Interest (ROI) is calculated using the Currie expression for the standard deviation of the background (Currie, 1968):

$$L_D = 2.71 + 3.29\sigma_B \quad (7)$$

where σ_B is the standard deviation of the background (natural plus intrinsic) measured in counts in the considered ROI. The background and σ_B were obtained with the filled vessel during a period of low count rates from natural origin (e.g. no precipitation present).

The width of the ROI is determined by the width of the expected peak, which is proportional to the $FWHM(E)$ function:

$$n = n(E) = \alpha \cdot FWHM(E) \quad (8)$$

where α is the proportionality constant to set the desired peak coverage and $FWHM(E)$ is obtained using Equation (2). In this study, $\alpha = 2.548$ for a 99.73% peak area coverage.

3.4 Data analysis discrimination criterion

The spectrometry monitors of the automatic real-time surveillance network of Catalonia provide new data every 10 min. In order to simplify the analysis task, a discrimination criterion was implemented to identify suspicious spectra. The total counts per second (cps) of each registered spectrum are counted, x_i , and the value is checked to be in the following interval:

$$\mu - k\sigma \leq x_i \leq \mu + k\sigma \quad (9)$$

where μ is the mean value of the total cps of spectra in a long period, σ the standard deviation and k a confidence factor.

If the value fails the established criterion, especially above the interval, the spectrum is analysed in detail. This criterion is used in all types of monitors of the Catalan radiological surveillance network with the confidence factor k set at 2 (Casanovas et al., 2011).

4 Results and Discussion

4.1 Energy and resolution calibrations

During the period analysed in this study, the water temperature variations were very low. However, the applied stabilisation method corrected the relative drift of the peaks that could be affected by temperature changes.

The energy calibration was carried out using an internally developed software for fitting Gaussian peaks using the Levenberg-Marquardt algorithm. The software provides the exact centre of the Gaussian and the corresponding FWHM in channels among many other parameters.

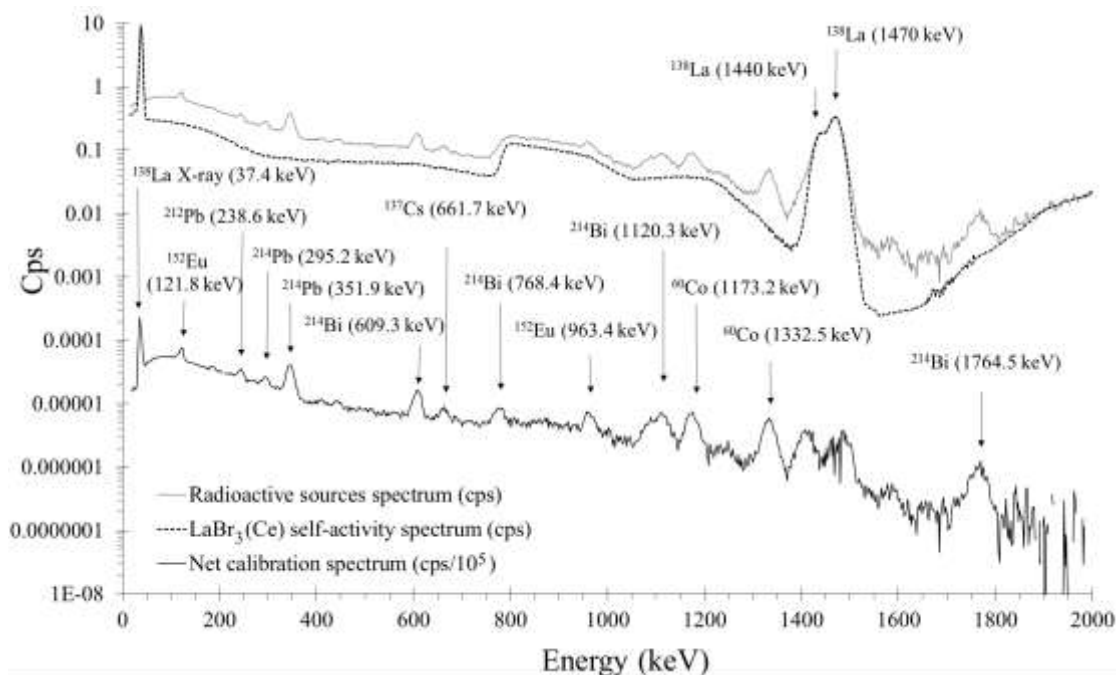


Figure 4. Spectra used for the energy calibration (black line). The Radioactive sources spectrum (grey line) and the $\text{LaBr}_3(\text{Ce})$ self-activity spectrum (dotted line) are shown in cps, whereas the Net calibration spectrum (black line) is shown in $\text{cps}/10^5$ for illustrative purposes. The main peaks of the used radioactive sources are labelled.

Figure 4 shows the spectra used for the energy calibration with the main peaks used. The grey line and the dotted line correspond to the radioactive sources spectrum and to the self-activity of the detector, respectively. Both spectra are shown in cps. Below them, the net calibration spectra (black) shows the radioactive source spectrum resulting from subtracting the intrinsic activity. It is presented in $\text{cps}/10^5$ for illustrative purposes. It is remarkable that the two peaks from the $\text{LaBr}_3(\text{Ce})$ self-activity at 1440 keV and 1470 keV are not well defined in the resulting net calibration spectrum. Thus, the information of the peaks position was taken from the radioactive sources spectrum and incorporated to the energy calibration. The subtraction of the detector self-activity is advantageous to distinguish hidden contributions, such as the 768.4 keV emission of ^{214}Bi , which is completely hidden by the gamma emission at 789 keV of ^{138}La and its associated beta continuum (Nicolini et al., 2007). However, this process incorporates some difficulties. For example, the temperature peak shift stabilisation and the energy calibration must be continuously checked for the acquired spectra in order to properly subtract the recorded self-activity spectra, as little variations between them could result in a misleading spectral analysis.

The energy calibration of the system is shown in Figure 5. Data used for the calibration were fitted to Equation (1) and gave a coefficient of determination of $R^2 = 0.99999$.

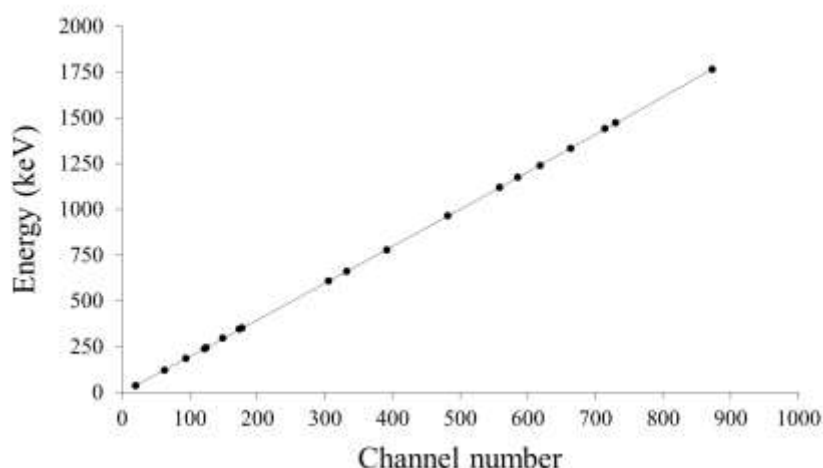


Figure 5. Energy calibration of the LaBr₃(Ce) detector. The solid line corresponds to the 2nd degree polynomial fit.

By way of example, the energy value obtained for the 661.7 keV photopeak of ¹³⁷Cs was 660.7 keV, which represents a relative difference of 0.15%. The maximum relative difference obtained in the energy calibration was 0.9% for the 238.6 keV photopeak of ²¹²Pb giving an energy of 240.8 keV, which corresponds to a 2.2 keV deviation.

The energy resolution of the system was determined using Equation (2), which resulted in a coefficient of determination $R^2 = 0.995$. The data used for the resolution calibration are drawn in Figure 6.

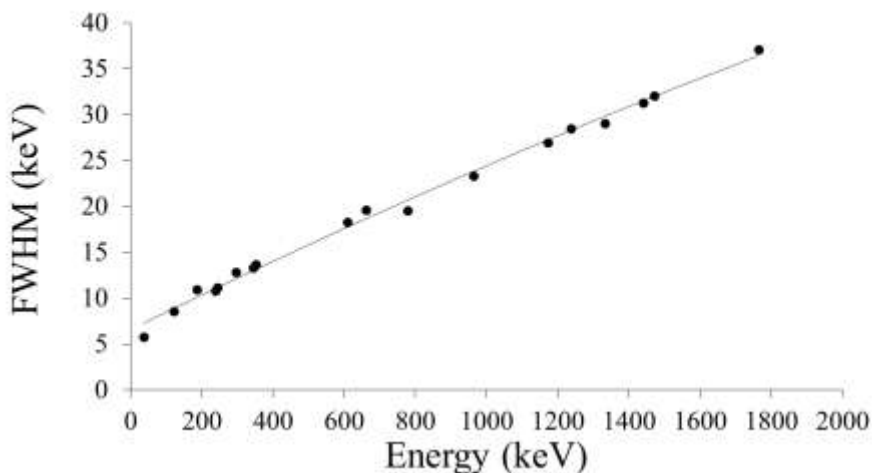


Figure 6. FWHM calibration of the LaBr₃(Ce) detector. The solid line corresponds to the 2nd degree polynomial fit.

The obtained FWHM curve is adequate for its purposes and the determination of the values was precise due to the resolution of the LaBr₃(Ce) detector crystal. At 661.7 keV, the FWHM obtained for ¹³⁷Cs is 19.6 keV, giving a resolution of 2.9%, which is similar to the value of 3% obtained for a 2''×2'' LaBr₃(Ce) detector (Quarati et al., 2007). In other studies, the resolution obtained for different LaBr₃(Ce) crystal sizes is also < 3%: 2.9% for a 3''×3'' crystal size (Saint-Gobain Crystals, n.d.) and 2.8% for a 1.5''×1.5'' crystal size (Iltis et al., 2006).

4.2 Efficiency calculation

The efficiency curve for the $\text{LaBr}_3(\text{Ce})$ water monitor obtained with MC simulations is drawn in Figure 7. In addition, the efficiency curve obtained for the water monitor with a $\text{NaI}(\text{Tl})$ detector in Casanovas et al. (2013) is shown for comparison purposes.

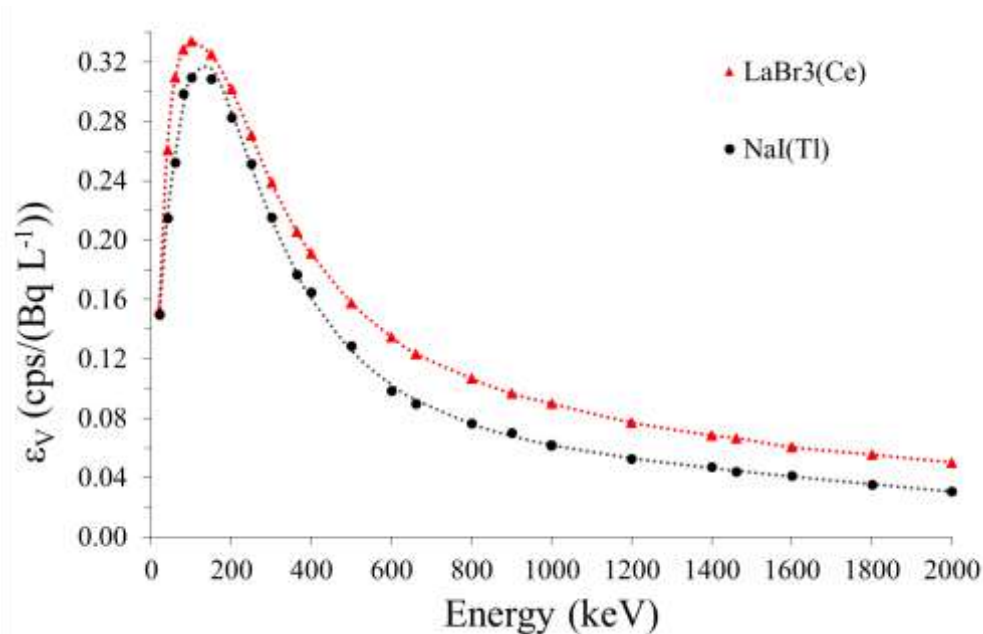


Figure 7. Efficiency curves obtained for the $\text{LaBr}_3(\text{Ce})$ water monitor (triangles) and for the $\text{NaI}(\text{Tl})$ water monitor (dots) calculated using MC simulations (Casanovas et al., 2013). The dotted lines correspond to the fitted curve given by equation (4).

Given that the water monitor is implemented for continuous surveillance, the water flows permanently through the shielded vessel. Therefore, it was not possible to fill the vessel with certified radioactive liquid sources and compare the simulated values with experimental results. However, the efficiency curve was obtained using an EGS5 MC user code previously validated for efficiency calculations (Casanovas et al. 2012).

The obtained values for the efficiency of $\text{LaBr}_3(\text{Ce})$ water monitor are higher than those obtained for the $\text{NaI}(\text{Tl})$ water monitor in all the energetic range (Figure 7). The quotient between efficiency values, $\varepsilon_{V_{\text{LaBr}}} / \varepsilon_{V_{\text{NaI}}}$, is close to 1 for low energies (below 250 keV) and near 1.4 for medium energies (from 600 keV to 1400 keV), which is in agreement to the value of the detector densities quotient, $\rho_{\text{LaBr}} / \rho_{\text{NaI}}$, where $\rho_{\text{LaBr}} = 5.3 \text{ g/cm}^3$ and $\rho_{\text{NaI}} = 3.7 \text{ g/cm}^3$. Thus, this was used as an acceptance criteria for the calculated values, as the $\text{NaI}(\text{Tl})$ ones were validated experimentally.

The efficiency values given by the simulation could not be strictly compared to those obtained in other studies with $\text{LaBr}_3(\text{Ce})$ detectors, due to the unique characteristics of the river water monitor vessel. Another study determined the efficiency for a 2'' \times 2'' sea water monitor using $\text{LaBr}_3(\text{Ce})$ detectors (Zeng et al., 2017) where the detector was placed in the middle of a sea water cylindrical tank of $\text{Ø}2.0 \text{ m} \times 2.3 \text{ m}$. The simulated results for a 2'' \times 2'' $\text{LaBr}_3(\text{Ce})$ detector gave a volumetric efficiency value of 0.0867 cps/(Bq L⁻¹) for ^{137}Cs (Zeng et al., 2017), which is lower than the efficiency computed in this work of 0.125 cps/(Bq L⁻¹).

4.3 MDAC

The minimum detectable activity concentrations were calculated for ^{131}I and ^{137}Cs , as these are typical isotopes that are susceptible of being released by the nuclear power plant in case of accident (Nuclear Energy Agency, 2002). MDAC values were calculated using equation (6) and are shown in Table 1. The widths of the ROI of the expected peaks were set with $\alpha = 2.548$ to obtain a 99.73% peak area coverage.

Time	MDAC (Bq L ⁻¹)	
	^{131}I	^{137}Cs
10 min	1.07	1.76
1 h	0.45	0.69
4 h	0.24	0.34
12 h	0.14	0.15
24 h	0.10	0.08

Table 1. MDAC values for ^{131}I and ^{137}Cs obtained for different integration times.

The self-activity of the $\text{LaBr}_3(\text{Ce})$ detector rises the values of the MDAC compared to the ones obtained with $\text{NaI}(\text{Tl})$ detectors (Su et al., 2011). Note that the MDAC results are independent from the intrinsic background and are only related to the dispersion of the background values, σ_B . Given that σ_B is higher in the monitor with a $\text{LaBr}_3(\text{Ce})$ detector, so are the calculated MDAC. By means of example, for ^{137}Cs , the MDAC calculated in the river monitor using a $\text{NaI}(\text{Tl})$ detector for 10 min was 0.6 Bq L⁻¹, whereas for $\text{LaBr}_3(\text{Ce})$ is 1.76 Bq L⁻¹.

4.4 Rainfall episode spectrum analysis

An episode of rainfall occurred during the period that the $\text{LaBr}_3(\text{Ce})$ detector was installed in the water monitor. Spectra were collected and analysed to check the calibration and the proper functioning of the monitor. Figure 8 shows the total (summed) number of counts per second (cps) of each acquired 10 min spectrum without the detector self-activity from 60 to 1980 keV (red dots) with the rain measures (blue line). The temporal coincidence of the rain with the increase of cps is clearly shown. The grey areas mark the periods that were analysed by spectrum analysis.

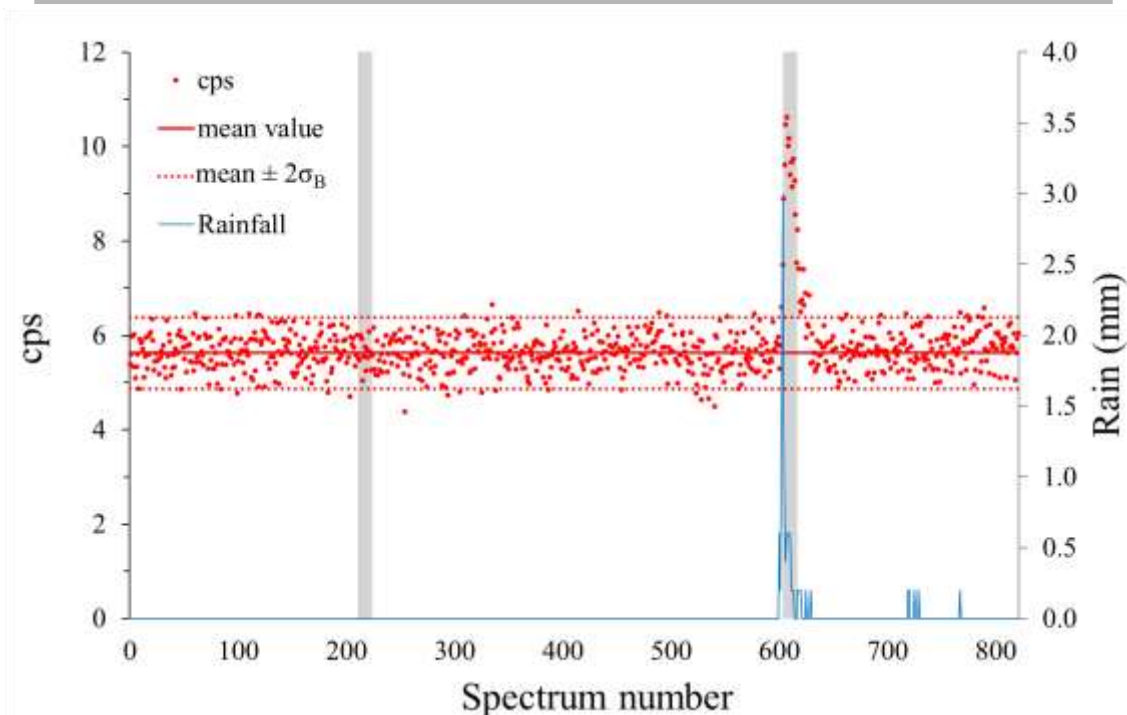


Figure 8. Radiological increments measured in cps (red dots), correlated with rainfall (blue line). The cps mean value (red line) with the statistical discrimination criterion (red dotted line) are added. The grey areas indicate the total spectra considered for the analysis, corresponding to the spectra shown in Figure 9. (For interpretation of the references to colour in this figure legend, the reader is referred to the web version of this article.)

Figure 9 shows two spectra, one obtained during rainfall (red) and another registered in a period without precipitation (black), which correspond to the areas marked in grey in Figure 8. Both spectra were obtained by summing all the 10 min spectra marked by the grey regions in Figure 8, which was equivalent to an integration time of 2 h and 10 min. The intrinsic self-activity of the detector crystal was removed in both spectra. It is worth mentioning that the shielded vessel of the water monitor attenuates a great amount of background radiation. And thus, the augments of the registered spectra with the $\text{LaBr}_3(\text{Ce})$ detector were very close to its self-activity spectrum during all the trial period, excluding the rain episode.

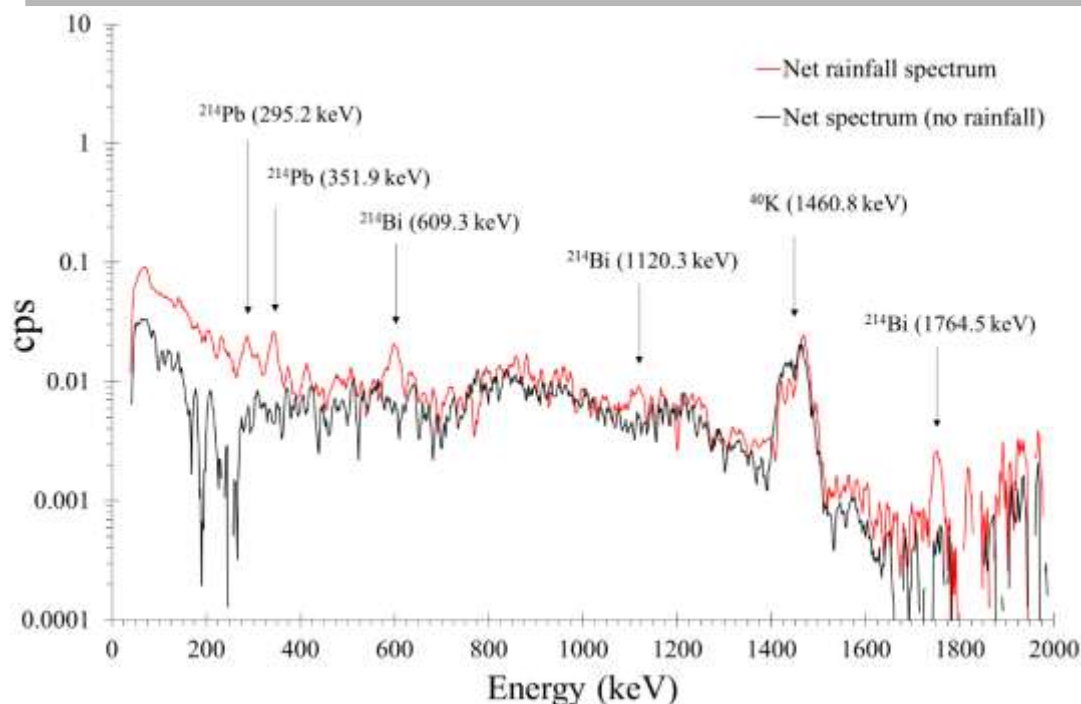


Figure 9. Rainfall spectrum without the detector self-activity (red) and background spectrum without the detector self-activity (black). Peaks of the identified isotopes are labelled. (For interpretation of the references to colour in this figure legend, the reader is referred to the web version of this article.)

In Figure 9, the peak located between 1400 and 1500 keV corresponds to the contribution from the emission of ^{40}K at 1460.8 keV, which is dissolved in the river water, plus the remains of the subtraction of the self-emission peaks of ^{138}La at 1440 keV and 1470 keV. Below 700 keV, some peaks corresponding to natural emissions can be identified, such as those from ^{214}Bi (609.3 keV, 1120.3 keV and 1764.5 keV) and ^{214}Pb (295.2 keV and 351.9 keV). The Compton contribution is remarkable below 400 keV.

The activity of ^{214}Bi was calculated using the 609.3 keV emission during the rain episode giving a value of 3.7 Bq L^{-1} . The counts under the 609.3 keV peak were determined subtracting the net spectrum from the net rain spectrum. The same activity calculation was performed for the South Ebre River Monitor with a NaI(Tl) detector for the same rain episode. The value obtained for ^{214}Bi was 3.4 Bq L^{-1} . In view of the results and attending that the efficiency calibration of the NaI(Tl) detector was validated experimentally, the efficiency calibration that was performed in this study for the $\text{LaBr}_3(\text{Ce})$ was considered to be acceptable.

4.5 Data analysis discrimination criterion

The maximum increase in cps (see Figure 8) during the rain episode for the $\text{LaBr}_3(\text{Ce})$ monitor was 10.6 cps, which corresponds with 5.0 cps over a 5.63 cps background mean value with a standard deviation $\sigma_{\text{LaBr}} = 0.38$ cps. For the NaI(Tl) monitor, the increase was of 3.5 cps over a 3.2 cps background with a standard deviation $\sigma_{\text{NaI}} = 0.08$ cps.

As the river water monitors are part of the radiological surveillance network of Catalonia, the spectra that surpass in total cps a statistical threshold are studied in detail (see Section 3.4). The spectra that are analysed in detail are those that surpass the threshold $\frac{\Delta N_{\text{cps}}}{2\sigma_B} > 1$, which can be fulfilled either with high cps increases or low values of σ . Considering the values presented for the two water monitors, the increase registered with both detectors exceeded the threshold,

giving $\frac{\Delta N_{cps_{LaBr_3}}}{2\sigma_{LaBr_3}} = 6.6$ and $\frac{\Delta N_{cps_{NaI}}}{2\sigma_{NaI}} = 21.9$. It should be noted that the cps variation was greater in the monitor with a $LaBr_3(Ce)$ detector than with the $NaI(Tl)$ one, but the increment was less notable due to the major dispersion of the background values compared to the monitor with $NaI(Tl)$. For that reason, the river water monitor with the $LaBr_3(Ce)$ detector requires of higher variations to surpass the statistical threshold established by the value of σ . Precisely, a measurement that barely passes the threshold in the $NaI(Tl)$ monitor should be 4.7 times greater to be statistically noticed with the $LaBr_3(Ce)$ one. The higher dispersion in the background values of the monitor with the $LaBr_3(Ce)$ detector could be due to its intrinsic activity.

A similar behaviour of the two monitors is found when studying a ROI centred at the 609.3 keV emission of ^{214}Bi . In both monitors, the widths of the ROIs were determined using Equation (8) with $\alpha = 2.548$ that gives a 99.73% peak area coverage. Figure 10 shows the evolution of the ^{214}Bi ROIs of $LaBr_3(Ce)$ and $NaI(Tl)$ before and during the rain episode.

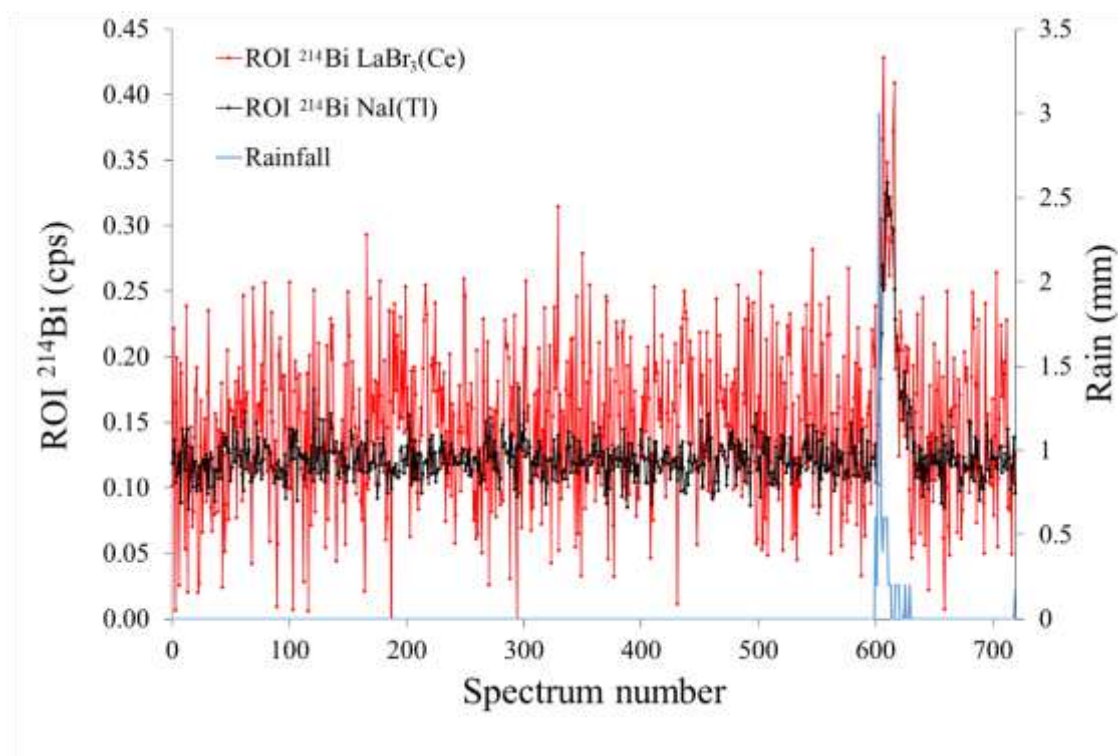


Figure 10. Cps registered in the ^{214}Bi ROI of the $LaBr_3(Ce)$ monitor (red) without its intrinsic background and $NaI(Tl)$ ^{214}Bi ROI (black), correlated with rainfall (blue line). (For interpretation of the references to colour in this figure legend, the reader is referred to the web version of this article.)

Table 2 shows the registered values of the ROIs drawn in Figure 10 during the rain episode along with the associated increment and threshold criterion for a 10 min integration time. Additionally, values for the monitor with a $NaI(Tl)$ detector are given in the same energetic range as the $LaBr_3(Ce)$ monitor ROI. This narrower $NaI(Tl)$ ROI would avoid possible counts from ^{137}Cs that could be included in the wider $NaI(Tl)$ ROI due the lower resolution of the $NaI(Tl)$ crystal.

	ROI range		Background (no rain)		Maximum value (rain episode)	Increment	
	E_{\min} (keV)	E_{\max} (keV)	μ_B	σ_B	N_{cps}	ΔN_{cps}	$\Delta N_{\text{cps}}/2\sigma_B$
LaBr ₃ (Ce)	587	632 ^a	1.96	0.057	2.25	0.29	2.5
NaI(Tl)	556	663 ^b	0.12	0.014	0.33	0.21	7.6
NaI(Tl)	587	632 ^a	0.05	0.009	0.20	0.15	8.2

^a Energy range corresponds to interval ($E_{609.3} \pm 2.548 \cdot \text{FWHM}_{\text{LaBr}_3(609.3)}$)

^b Energy range corresponds to interval ($E_{609.3} \pm 2.548 \cdot \text{FWHM}_{\text{NaI}(609.3)}$)

Table 2. Values of ²¹⁴Bi ROI cps registered during the rain episode compared to background. Increments and threshold criterion are given for both types of detectors.

As can be observed in Table 2, the total increment in counts of the ²¹⁴Bi ROI is still greater in the LaBr₃(Ce) monitor than in the NaI(Tl) one and the dispersion of the background is more than 4 times greater in the LaBr₃(Ce) monitor. Moreover, the ratio of the total cps increment to the background dispersion is still more than 3 times higher in the NaI(Tl) monitor. It is worth noting that the intrinsic background value of the ²¹⁴Bi ROI in the LaBr₃(Ce) monitor from the self-activity spectrum is 1.83 cps, which is close to the value obtained before the rain episode (1.96 cps).

Even if the better resolution of LaBr₃(Ce) allows us to determine a narrower ROI, there is little difference between the two ROIs of ²¹⁴Bi implemented for the NaI(Tl) monitor, as both of them behave similarly when compared to the LaBr₃(Ce) monitor, giving higher values of $\frac{\Delta N_{\text{cps}}}{2\sigma_B}$ than LaBr₃(Ce) in both cases.

5 Conclusions

A real-time gamma-ray spectrometry river water monitor was fully calibrated for operating with a 2"×2" LaBr₃(Ce) detector. After the experimental energy and FWHM calibrations together with the MC simulated efficiency computations, the monitor was ready to provide spectra suitable for carrying out isotopic analysis of the river water. Therefore, the water monitor with a LaBr₃(Ce) detector is adequate to quantify and identify radionuclides due to the good characteristics of its crystal (resolution, efficiency, density, linearity, etc.). However, the higher dispersion of the background values compared to the monitor with NaI(Tl) implies that a signal should be much greater to surpass the statistical criterion used in the Catalan network, which is related to the standard deviation of the background measurements. Thus, despite the greater dispersion, the water monitor with a LaBr₃(Ce) detector would be a better choice when spectra are registered in high count rate scenarios, where the counts of the measured spectra are remarkably superior to the intrinsic background of the detector. In the other hand, the use of a NaI(Tl) detector in the water monitor could be convenient to assure radiological quality in low count rate situations.

References

- Berger, M., Coursey, J., Zucker, M., Chang, J., 2005. ESTAR, PSTAR, and ASTAR: Computer Programs for Calculating Stopping-Power and Range Tables for Electrons, Protons, and Helium Ions (version 1.2.3) [WWW Document]. URL <https://www.nist.gov/pml/stopping-power-range-tables-electrons-protons-and-helium-ions>
- Casanovas, R., Morant, J.J., López, M., Hernández-Girón, I., Batalla, E., Salvadó, M., 2011. Performance of data acceptance criteria over 50 months from an automatic real-time environmental radiation surveillance network. *J. Environ. Radioact.* 102, 742–748. doi:10.1016/j.jenvrad.2011.04.001
- Casanovas, R., Morant, J.J., Salvado, M., 2014a. Development and calibration of a real-time airborne radioactivity monitor using gamma-ray spectrometry on a particulate filter. *IEEE Trans. Nucl. Sci.* 61, 727–731. doi:10.1109/TNS.2014.2299715
- Casanovas, R., Morant, J.J., Salvadó, M., 2014b. Development and calibration of a real-time airborne radioactivity monitor using direct gamma-ray spectrometry with two scintillation detectors. *Appl. Radiat. Isot.* 89, 102–108. doi:10.1016/j.apradiso.2014.01.026
- Casanovas, R., Morant, J.J., Salvadó, M., 2013. Implementation of gamma-ray spectrometry in two real-time water monitors using NaI(Tl) scintillation detectors. *Appl. Radiat. Isot.* 80, 49–55. doi:10.1016/j.apradiso.2013.06.003
- Casanovas, R., Morant, J.J., Salvadó, M., 2012a. Temperature peak-shift correction methods for NaI(Tl) and LaBr₃(Ce) gamma-ray spectrum stabilisation. *Radiat. Meas.* 47, 588–595. doi:10.1016/j.radmeas.2012.06.001
- Casanovas, R., Morant, J.J., Salvadó, M., 2012b. Energy and resolution calibration of NaI(Tl) and LaBr₃(Ce) scintillators and validation of an EGS5 Monte Carlo user code for efficiency calculations. *Nucl. Instruments Methods Phys. Res. Sect. A Accel. Spectrometers, Detect. Assoc. Equip.* 675, 78–83. doi:10.1016/j.nima.2012.02.006
- Currie, L. a., 1968. Limits for qualitative detection and quantitative determination. Application to radiochemistry. *Anal. Chem.* 40, 586–593. doi:10.1021/ac60259a007
- Iltis, A., Mayhugh, M.R., Menge, P., Rozsa, C.M., Selles, O., Solovyev, V., 2006. Lanthanum halide scintillators: Properties and applications. *Nucl. Instruments Methods Phys. Res. Sect. A Accel. Spectrometers, Detect. Assoc. Equip.* 563, 359–363. doi:10.1016/j.nima.2006.02.192
- Mattila, A., Toivonen, H., Vesterbacka, K., Leppänen, M., Salmelin, S., Pelikan, A., 2010. Radiation monitoring network with spectrometric capabilities: implementation of LaBr₃ spectrometers to the Finnish network, in: *Proceedings of the Third European IRPA Congress. Helsinki, pp. 1958–1966.*
- Menge, P.R., Gautier, G., Iltis, A., Rozsa, C., Solovyev, V., 2007. Performance of large lanthanum bromide scintillators. *Nucl. Instruments Methods Phys. Res. Sect. A Accel. Spectrometers, Detect. Assoc. Equip.* 579, 6–10. doi:10.1016/j.nima.2007.04.002
- Nicolini, R., Camera, F., Blasi, N., Brambilla, S., Bassini, R., Boiano, C., Bracco, A., Crespi, F.C.L., Wieland, O., Benzoni, G., Leoni, S., Million, B., Montanari, D., Zalite, A., 2007. Investigation of the properties of a 1“x1” LaBr₃:Ce scintillator. *Nucl. Instruments Methods Phys. Res. Sect. A Accel. Spectrometers, Detect. Assoc. Equip.* 582, 554–561. doi:10.1016/j.nima.2007.08.221

- Nuclear Energy Agency, 2002. Assessment of Radiological and Health Impacts 2002 Update of Chernobyl : Ten Years On. Chernobyl, Assess. Radiol. Heal. Impacts.
- Quarati, F., Bos, A.J.J., Brandenburg, S., Dathy, C., Dorenbos, P., Kraft, S., Ostendorf, R.W., Ouspenski, V., Owens, A., 2007. X-ray and gamma-ray response of a 2"x2" LaBr₃:Ce scintillation detector. Nucl. Instruments Methods Phys. Res. Sect. A Accel. Spectrometers, Detect. Assoc. Equip. 574, 115–120. doi:10.1016/j.nima.2007.01.161
- Quarati, F.G.A., Khodyuk, I. V., Van Eijk, C.W.E., Quarati, P., Dorenbos, P., 2012. Study of ¹³⁸La radioactive decays using LaBr₃ scintillators. Nucl. Instruments Methods Phys. Res. Sect. A Accel. Spectrometers, Detect. Assoc. Equip. 683, 46–52. doi:10.1016/j.nima.2012.04.066
- Saint-Gobain Crystals, n.d. BrillLanCe™ Scintillators Performance Summary (Revision: January, 2009).
- Su, G., Zeng, Z., Cheng, J., 2011. Monte carlo simulation of in situ LaBr gamma-ray spectrometer for marine environmental monitoring. Radiat. Prot. Dosimetry 146, 103–106. doi:10.1093/rpd/ncr122
- Toivonen, H., Vesterbacka, K., Pelikan, A., Mattila, A., Karhunen, T., 2008. LaBr₃ Spectrometry for Environmental Monitoring, in: Proceedings of the 12th International Congress of the International Radiation Protection Association. Buenos Aires.
- Zeng, Z., Pan, X., Ma, H., He, J., Cang, J., Zeng, M., Mi, Y., Cheng, J., 2017. Optimization of an underwater in-situ LaBr₃:Ce spectrometer with energy self-calibration and efficiency calibration. Appl. Radiat. Isot. 121, 101–108. doi:10.1016/j.apradiso.2016.12.016

Highlights

- A 2"x2" LaBr₃(Ce) gamma-ray spectrometry water monitor is characterized.
- Experimental energy and resolution calibrations are performed.
- The detector efficiency is obtained by MC simulations with EGS5 code system.
- Minimum detectable activity concentrations for ¹³¹I and ¹³⁷Cs are given.
- A rainfall radiological increment is compared with the NaI(Tl) monitor.